# Natural and human influences on Central England Temperature

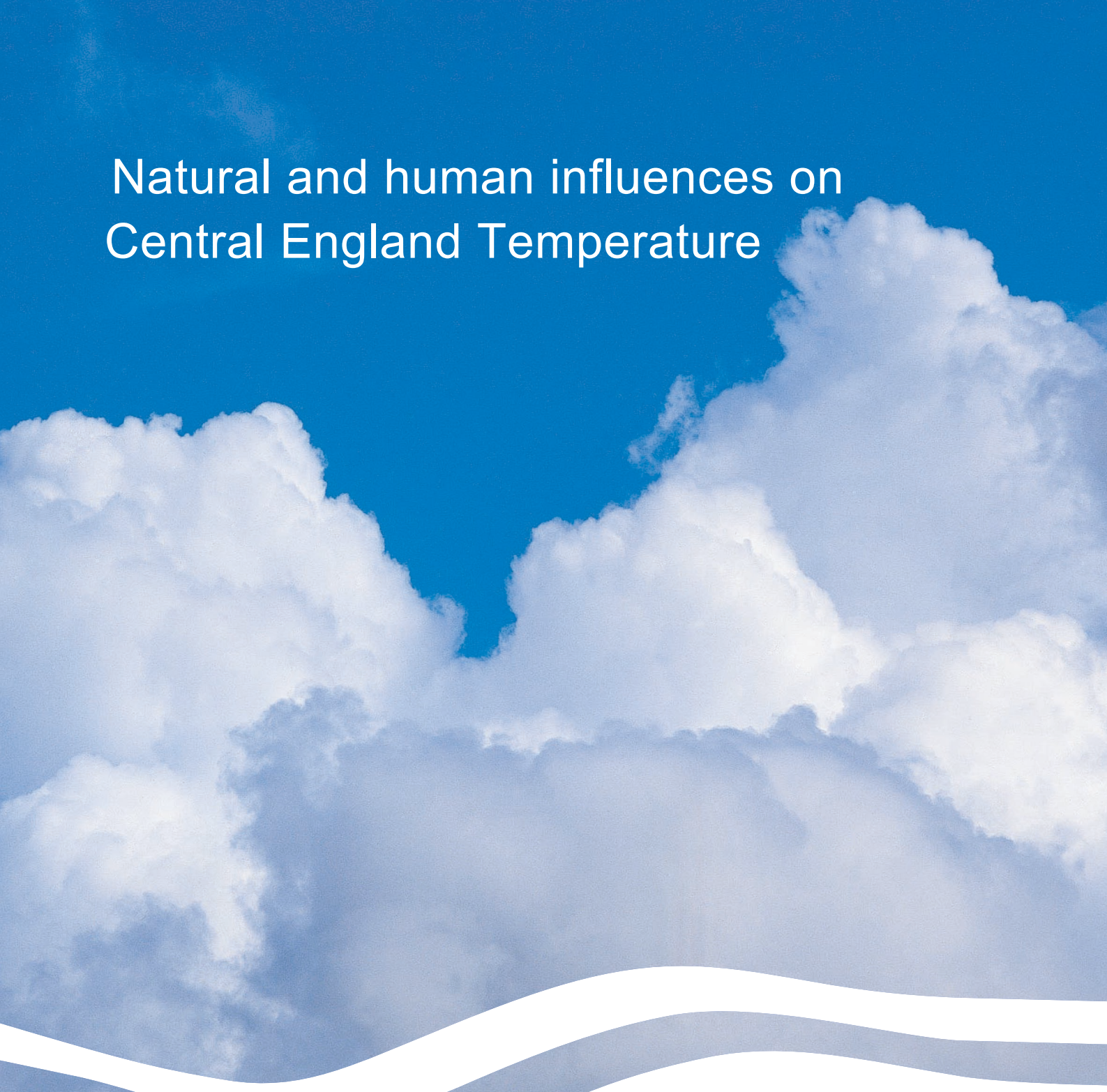

Hadley Centre technical note 46

*David M H Sexton, David E Parker, and Chris K Folland*

January 2004

# Natural and human influences on Central England Temperature

David M H Sexton, David E Parker, and Chris K Folland

Hadley Centre, Met Office, Bracknell, U.K.

Corresponding author address: David M. H. Sexton, Hadley Centre for Climate Prediction and Research, Met Office, Fitzroy Road, Exeter, Devon, EX1 3PB, UK;
Email: David.Sexton@metoffice.com

**Abstract**

Daily Central England temperature (CET) since 1881 is analysed to assess the influences of regional atmospheric circulation, regional sea surface temperature (SST), urban warming, and increasing greenhouse gases and tropospheric aerosols. Although regional atmospheric circulation changes have not greatly influenced trends in CET since 1881, they have contributed approximately half of the warming in the winter half-year since 1966. We show that the CET series is free from a warming bias due to urban development. An atmospheric general circulation model, HadAM3, forced with observed SST and natural forcings quite skilfully reproduces many of the variations of CET. These notably include multidecadal periods of both cooling and warming. The fit to multi-decadal variations of CET is further improved if increasing greenhouse gas concentrations are also explicitly included, although there is only just sufficient data to show this. Tests show that this is unlikely to be because the observed effect of local circulation changes on CET is mistakenly being explained by the modelled response to anthropogenic radiative forcing. From this, we infer a probable human contribution to climate change in the U.K.

## 1. Introduction

The evidence for human influence on climate change during the last century is mounting steadily (e.g. Houghton et al. 2001). Much of this evidence is based on detection and attribution studies that investigate changes in surface temperature on the global scale (e.g. Stott et al. 2000; Tett et al. 1999). Recently, studies have broadened the search for an anthropogenic signal on climate to large sub-global scales such as hemispheric (e.g. Braganza et al. 2003) and continental (e.g. Stott 2003; Zwiers and Zhang 2003). Zwiers and Zhang (2003) conclude that this increased effort towards detection of climate change at regional scales will prompt policy makers to appreciate that we face a local, not just a global problem. Accordingly, there is a desire to understand climate change at a national scale (e.g. Spagnoli et al. 2002) and so in this study we assess the underlying causes of temperature changes in the UK since 1881.

However, Stott and Tett (1998) suggest that detection results based on coupled ocean-atmosphere GCM integrations are only applicable at spatial scales greater than 2000km. To overcome this problem, Folland et al. (1998) and Sexton et al. (2001) use atmosphere-only GCM integrations with prescribed historical oceanic changes, and natural and anthropogenic radiative forcings to simulate climate change from 1871. Due to the inclusion of observed changes in SST, climate variability in atmosphere-only GCM integrations is more realistic at smaller spatial scales than their coupled ocean-atmosphere counterparts. However, a large part of the anthropogenic signal is already contained in the prescribed changes in SST and sea-ice extent and so these runs cannot be used to estimate the total anthropogenic contribution to climate change. Nevertheless, this experiment can be used to show that the inclusion of anthropogenic radiative forcings in addition to prescribing variations at the ocean surface in the atmosphere-only GCM is required to simulate recent climate change, thereby indicating that human activities have played some role in recent climate change.

We use a similar approach to Folland et al. (1998), although the experimental design has been improved so that the contributions of the radiative forcings can be more easily diagnosed (Sexton et al. 2003). We consider the effects on Central England Temperature (CET) of possible urban warming, regional SST, increasing greenhouse gases, changing tropospheric and stratospheric ozone and tropospheric aerosols. We also consider the effects of regional atmospheric circulation variations, as there have been strong variations of climate over the North Atlantic over the last century, involving, for example, the North Atlantic

Oscillation in winter (Hurrell, 1995) and regional atmospheric circulation in summer (Hurrell et al. 2001). One GCM has shown that the recent trend in NAO may be a response to increasing greenhouse gases (Shindell et al., 1999). However, the GCM we use in this study, HadAM3, shows no such response. Therefore, we use a similar approach to Osborn and Jones (2000) to factor out the mean effect of atmospheric circulation on CET. To quantify the relationships between atmospheric circulation over the UK and CET, Osborn and Jones (2000) used regression with explanatory variables of wind direction, speed and vorticity estimated objectively from daily gridded mean sea level pressure fields (Jones et al. 1993). We present an alternative, more powerful method for quantifying these relationships. The technique, *locally weighted regression* (sometimes called *lowess*) allows for the complex non-linear interactions between these three properties of the atmospheric circulation. Lowess is applied to estimate the effects of atmospheric circulation on both modelled and observed data. As our methodology for extracting the circulation influence from CET is new, we re-assess the CET trend analysis of Osborn and Jones (2000). We also use the atmospheric circulation data to assess the freedom of CET from urban bias by comparing trends of CET on nights with light winds, when urban influences are strongest (Johnson et al. 1991), with trends on windier nights when they are minimal.

## 2. Data processing

### *a. Treatment of observations*

The daily record of observed maximum, minimum and mean CET is based on three or four stations with standard thermometer exposure since 1878 (Parker et al. 1992). These data have been converted to anomalies by subtracting the climatological normal for each day. Daily twentieth century normals were estimated by smoothing raw daily averages for 1900-1998 with a low-pass filter having a half-power near 8.5 days (Jones et al. 1999).

### *b. Treatment of model simulations*

Initial results were based on three ensembles of simulations by the Hadley Centre atmospheric general circulation model (AGCM) HadAM3 which has a horizontal resolution of 2.5° latitude x 3.75° longitude (Pope et al. 2000). Each ensemble was forced with historical SST and sea-ice concentrations from the Hadley Centre Global sea-Ice and Sea Surface Temperature (GISST3.1) data set (updated from Rayner et al. 1996). Ensemble SSTNAT, with 6 members, ran from 1880 to 1998 and was also forced with changes in stratospheric

aerosol concentrations from volcanic eruptions (Sato et al. 1993) and in solar total irradiances (Lean et al. 1995). Ensemble GSOT, with 4 members, ran from 1900 to 1998 and included natural forcings and a set of anthropogenic forcings due to well-mixed greenhouse gases, tropospheric and stratospheric ozone, and the direct cooling effects of tropospheric sulphate aerosols formed from man-made emissions of sulphur dioxide. Ensemble GSOTI, with two members until 1949 (owing to computing restraints) and 6 members thereafter, also ran from 1900 to 1998, and included the same natural and anthropogenic forcings plus the estimated indirect cooling effects of tropospheric sulphate aerosols (Johns et al. 2001), which is due to enhanced cloud albedo. We did not include the possibly offsetting warming effects of soot and other low-albedo particles. Simulated CET was defined as the average 1.5m temperature at four model grid points weighted to represent 52.6°N, 1.5°W. Daily maxima and minima were calculated as the highest and lowest of the 48 half-hourly simulated values beginning at midnight. Daily mean CET was estimated as the average of the daily maximum and minimum CET values. Anomalies were generated using smoothed daily 1900-1998 climatological averages calculated from one member of SSTNAT. By basing model and observed anomalies on their respective daily climatologies, we largely remove model biases.

## 3. Estimation of the influence of atmospheric circulation on CET

Osborn et al. (1999) used geostrophic wind direction, speed, and vorticity to predict the mean influence of atmospheric circulation on daily CET anomalies; these three properties of the flow were estimated from sea level pressure fields produced by operational analyses using the method of Jenkinson and Collison (1977). First, Osborn et al. estimated the individual effects of each air flow index, allowing for any non-linear relationships with CET by dividing the range of each flow index into 20 intervals and estimating the mean effect for each of those intervals. Osborn et al. showed that all three indices were important in determining CET throughout most of the year, with wind direction having the largest effect. Osborn et al. also produced a bivariate estimate of the combined effect of wind direction and speed on CET by dividing these two indices into 10 intervals and estimating the mean effect for each of the 10x10=100 bins. They found that speed and wind direction interacted non-linearly so that the combination of their two univariate analyses produced a poor prediction of the mean circulation effect on CET, particularly for easterly flow. Although their bivariate estimate accounts for non-additive interactions between two air-flow indices, the observations are spread over 100 bins rather than the 20 used in the univariate analysis, so that the estimated

mean effects are less robust. The problem would be exacerbated if all three indices were used and predictions based on such an analysis would be useless. Therefore, Osborn et al. predicted the mean effect from all three indices by assuming that the overall effect was a linear combination of the individual effects, an assumption that was not validated.

We use *locally weighted regression* or *lowess* to fit a smooth regression surface to the data. Lowess takes into account the effect of all three air-flow indices, allowing for the non-linear interactions between the three effects. This is an improvement over estimating the mean effect in each interval, in a similar way that low-pass filtering of annual data is better than the corresponding decadal mean time series. Section a of the Appendix briefly explains the essential properties of the lowess technique, but a more detailed account is given by Cleveland and Devlin (1988). This method has three advantages over the techniques used in Osborn et al. (1999):

1. The effects of all three flow indices can be fitted simultaneously, and there is no need to assume that the combined response has some linear relationship to the individual effects.

2. By fitting a surface to the data, lowess effectively uses fewer degrees of freedom to describe the variations in the data and therefore provides a more precise predicted effect. The effective number of parameters, $N_p$, is determined by the lowess algorithm. It is essentially a measure of how smooth the response is as a function of the three flow indices; A smoother response can be fitted using fewer degrees of freedom.

3. Two different lowess models can be compared to see which model best explains the variations in the data. Therefore, we can objectively determine the fraction of the data that defines 'local' and/or the optimum number and degree of indices to use in the analysis. In contrast, the choice of the number of intervals used in the analysis of Osborn et al. (1999) is purely subjective.

Lowess estimates the combined effect of the three flow indices for each datum by fitting a multivariate polynomial regression to a fraction (the '*span*') of the data that is 'local' to that datum. We applied lowess month by month rather than season by season (Osborn et al. 1999). The polynomial regression may be either linear (degree 1) or quadratic (degree 2) and the degree can be different for each variable. For this analysis, we chose a locally linear fit for speed and vorticity but a locally quadratic effect for direction and its interactions with speed

and vorticity. This choice was made because quadratic fits are very sensitive to outliers and we wanted to avoid any such behaviour for large values of speed and vorticity. For wind direction, we used an objective test to show that the locally quadratic fit explained a significantly larger amount of variation in the data than the locally linear fit. Normally, lowess does not deal with cyclic variables and so does not treat wind directions close to $0^o$ and $360^o$ as being 'local'. Therefore, we adapted the lowess routine to approximately account for the cyclic nature of wind direction (see section a in the Appendix), to improve the fitting near $0^o$ and $360^o$.

The lowess estimate is not unique as the *span* can be varied. Mallow's $C_p$ statistic (Cleveland and Devlin 1988) was used to guide the choice of *span* and to determine the combination of variables to use. We found that vorticity was required to predict the effect of circulation on the CET anomalies in the model for all months, but only in December for the observations. However, as we wanted to use the same span and variables for the analysis of both modelled and observed data, we included vorticity in the observational analysis. We used a span of 20% for all months, despite results from Mallow's $C_p$ test which showed that 30-40% was adequate for most months. Comparisons of the lowess regression surfaces with spans of 20% (see Fig. 1), 30% and 40% (not shown) showed that the larger spans smoothed the lowess fits too much; thus certain known sharply varying effects of relatively small variations in wind direction on CET (e.g. near southerly in winter) were missed. The assumptions of lowess are that the residual variations are Gaussian with constant variance. Inspection of the residuals revealed this to be largely true, although the residuals had an extended negative tail for January and a positive tail for July and August. In winter, this mainly occurs in anticyclonic situations when the source of the air mass has not been adequately accounted for by wind direction. In summer, large positive residuals can occur when a change of air mass at the end of a heat wave is associated with warm, cloudy nights. The variance was constant for the majority of residuals although spread of the residuals could change for a very few extreme speeds and vorticities. Local regression fits are unlikely to be affected by serial correlation in time because each local fit in the lowess procedure is likely to be based on a fraction of the data that are spread out over the period 1900-1998 and so are mostly separated in time.

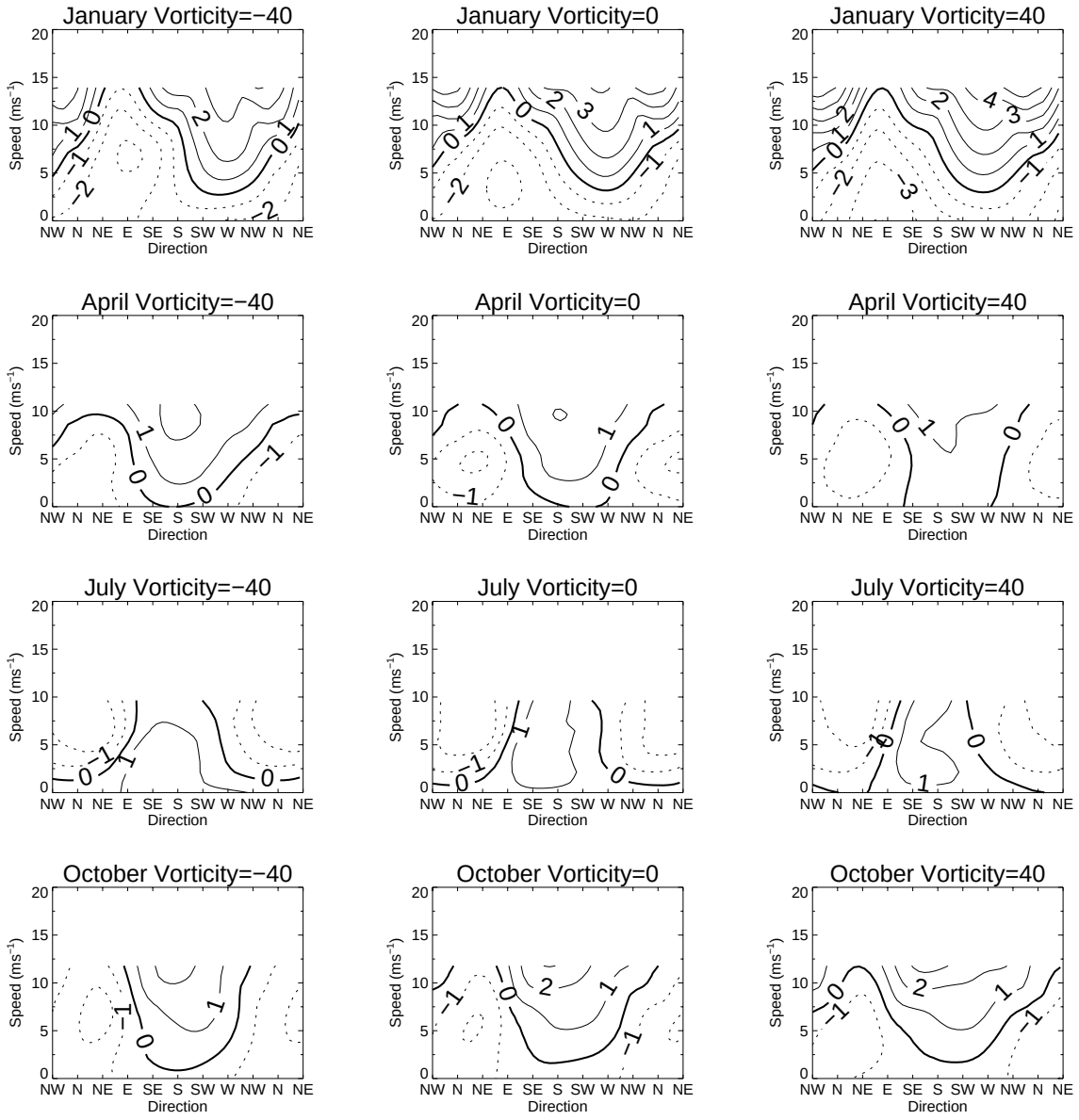


**Figure 1**. *Mean effect of wind direction and speed on observed daily mean CET ($^oC$) for three values of vorticity and for January, April, July and October. The smooth regression surface estimated by lowess was sampled for 1ms$^{-1}$ intervals of speed and 40 equally-spaced values for wind direction.*

In situations with neutral vorticity, there are clear non-linear interactions between wind direction and speed (see Fig. 1). For instance, in January strong easterlies are only slightly warmer than light easterlies whilst strong westerlies are several degrees warmer than light westerlies. This is an example of when a simple linear combination of the effects of two air-flow indices would not be appropriate. Fig. 1 shows that the combined effect of wind direction and speed on daily CET is altered by the vorticity of the air flow, particularly in

winter and spring. This mainly occurs in very windy conditions, which are not frequent enough to produce a strong effect from vorticity on observed CET.

Fig. 2a shows that the mean effect of circulation is greatest in February, explaining 33% of the variance in daily mean CET anomalies, whilst it is lowest in October. This is mainly due to the regional circulation effect on daily maximum CET, which is much larger than that on daily minimum CET. The number of effective parameters (see Fig. 2b) used in the lowess fit for each month is roughly constant as the same span of 20% is used throughout the annual cycle.

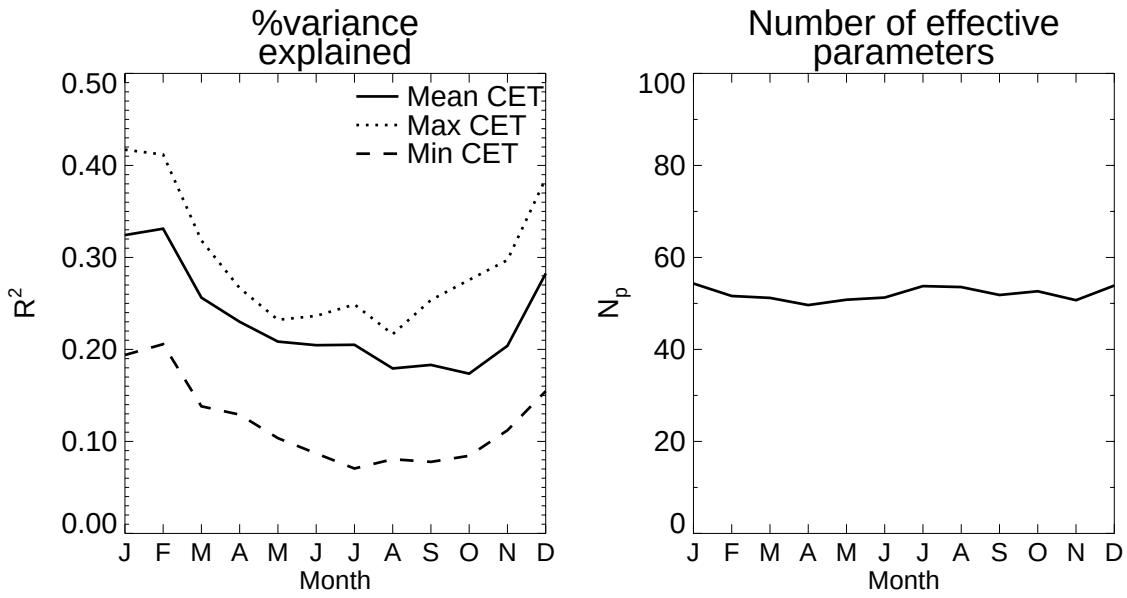


**Figure 2**. *Fraction of variance of observed daily maximum, minimum and mean CET explained by circulation (left panel) and the number of effective parameters used (right panel) as a function of calendar month, which is the same for the three variables.*

## 4. Observed CET trends

### *a. The effect of regional atmospheric circulation on observed CET trends*

CET anomalies and residuals were averaged over each year, season (December to February etc.), each winter half-year (October to March), each summer half year (April to September) and each high summer (July and August). High summer CET was analysed owing to strong recent warming in CET in that season.

Table 1 shows that regional atmospheric circulation changes have accounted for approximately half of the warming in the winter half-year since 1966. The warming trends of

the minimum CET residuals are about 55% smaller than those of the anomalies (see Table 1) and circulation effects account for 45% of the maximum CET trends. In the summer half year, regional circulation changes have not contributed to the statistically significant warming since 1966, although a fifth of the CET trend in high summer can be attributed to changes in circulation since that date. This approximately corresponds to an onset of increasingly anticyclonic conditions (Hurrell et al. 2001), also shown for July to September by Rodwell and Folland (2003).

**Table 1**. *Observed trends ($^{o}$C/decade) for the period 1966-2001 estimated by least squares regression allowing for 1$^{st}$ order autocorrelation. Bold values are significant at the 5% level.*

| | Minimum CET | | Maximum CET | |
|---|---|---|---|---|
| | Anomaly | Residual | Anomaly | Residual |
| Annual | .14 | .08 | **.34** | **.26** |
| Winter half | .18 | .08 | .34 | .18 |
| Summer half | .11 | .11 | **.36** | **.37** |
| High Summer | .14 | .11 | .56 | .46 |
| MAM | .31 | .28 | **.53** | **.48** |
| JJA | .08 | .08 | .34 | .33 |
| SON | .10 | .10 | .20 | .22 |
| DJF | .12 | -.08 | .33 | .06 |

Since 1881, regional atmospheric circulation changes have, overall, had little effect on trends of CET. For example, trends of anomalies and residuals of daily mean CET for the year as a whole for 1881-2001 were both 0.071°C/decade. Fig. 3 shows that the largest effect of circulation on multi-decadal fluctuations of CET over the period 1881-2001 has been during the winter half year. In particular, there was a large warming due to circulation during the late 1980s and early 1990s due to enhanced winter westerly circulation. In the 1960s winter temperatures were lowered by increased blocking and cold easterly winds from the Eurasian continent (Folland 1983). As shown by Table 1, multi-decadal changes in daily maximum CET dominate changes in the daily mean CET on those time scales.

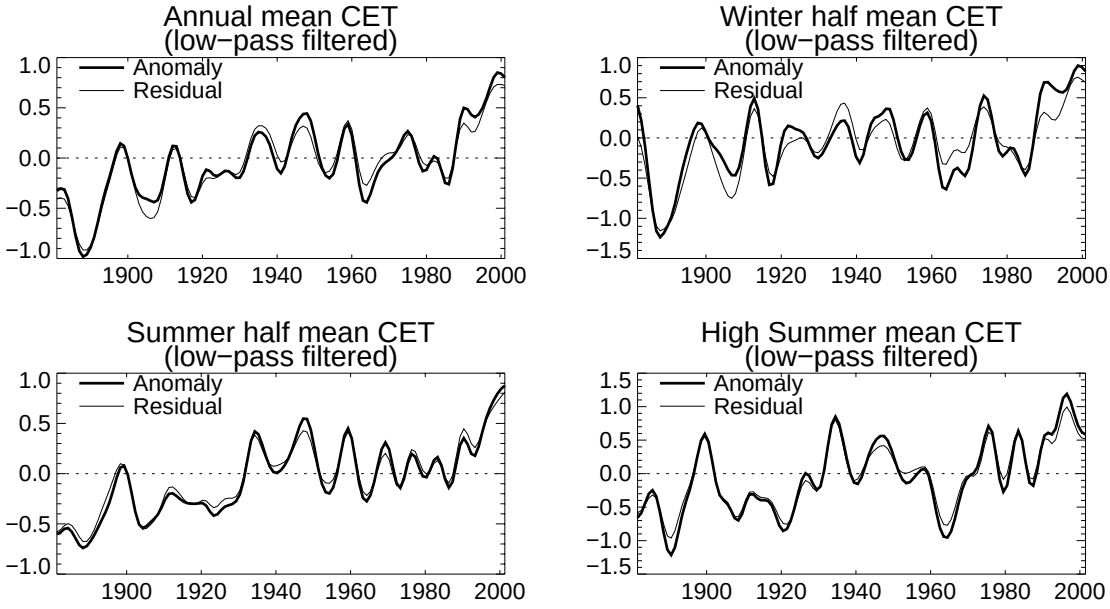


**Figure 3**. *Observed low-pass filtered (half power about 10 years) anomalies (heavy) and residuals (light) of daily mean CET (°C).*

*b. Trends in day versus night CET*

For 1950-1993, Easterling et al. (1997) used a set of non-urban station temperatures to estimate warming trends for the Northern Hemisphere of 0.077 °C/decade for day maximum temperatures and 0.17°C/decade for night minimum temperatures The maps in Easterling et al. (1997) show relative daytime warming over the UK, in opposition to the relative night-time warming trends over most continental regions. Over the same period annual-average maximum and minimum CET had trends of 0.089 and 0.036°C/decade respectively, both of which were not statistically significant.

*c. Trends in CET residuals on windy and light-wind days*

To seek for an urban warming signal, we estimated the trend in CET residuals on light-wind days and nights (geostrophic wind speed in lowest tercile) relative to windy days and nights (geostrophic wind speed in highest tercile). CET already includes some recent calendar monthly urban warming adjustments of up to 0.2$^{o}$C (Parker et al. 1992) but these will not affect trends on windy relative to calm days or nights. This is because the adjustments are to monthly means and thus do not distinguish between these conditions. If urban warming were significantly biasing the unadjusted CET, there would be stronger warming on calm nights than on windier nights (Johnson et al. 1991). However, minimum CET residuals on light-wind

nights since 1881 have not warmed relative to those on windy nights (Figure 4). So we conclude that the CET record overall since 1881 is unbiased by urban warming. A requirement for small adjustments of up to –0.2°C since 1980 (Parker et al. 1992) is not evident from these results, probably because of the substantial natural, interannual variation of (calm minus windy) CET residuals (not shown). There is a significant warming trend in maximum CET anomalies on calm days relative to windy days, but this is not a recognised symptom of urban warming. There are also no significant trends in the seasonal temperatures on calm days relative to windy days (Figure 4).

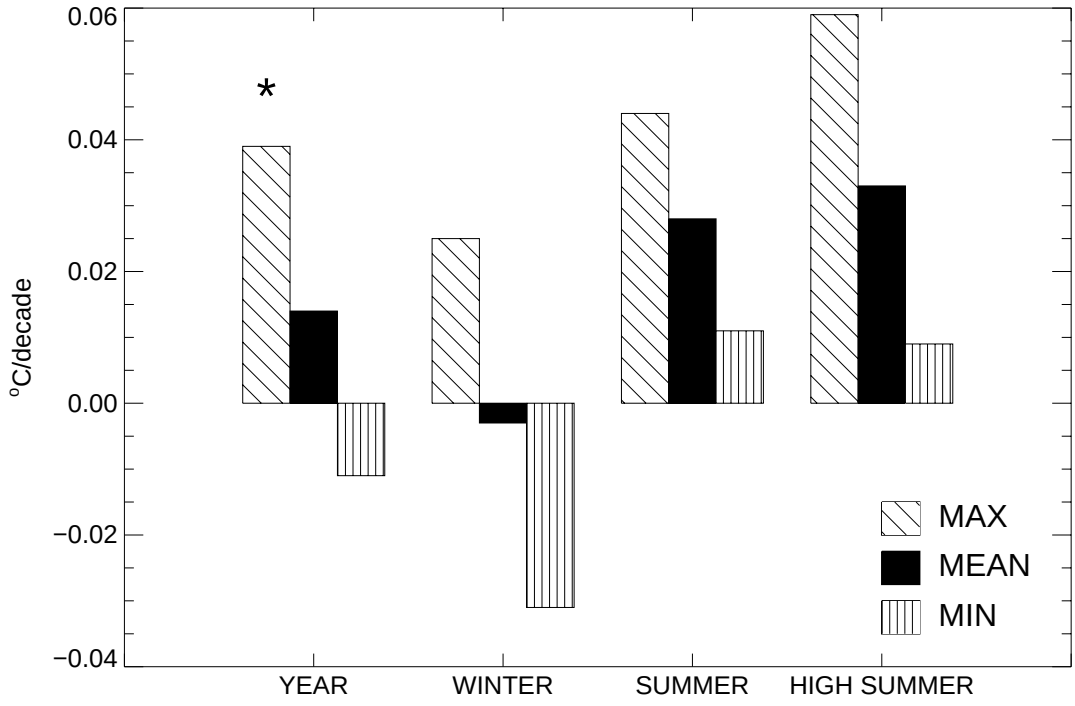


**Figure 4**. *Trends (°C/decade) in observed CET residuals, light-wind minus windier conditions, 1881-2001. Asterisk: significance at 5% level.*

## 5. Initial comparison of observed and simulated trends of CET

First we show how well the model simulates the characteristics of atmospheric circulation over the UK. For brevity, we restrict the analysis to daily mean CET. The lowess predictions for the model were based on CET anomalies and atmospheric circulation indices from the second member of SSTNAT over the period 1900-1998; the flow indices were calculated in the same way as the observations using mean sea level pressure data interpolated onto the observational grid. Fig. 5 shows that the climate model generally has stronger winds on average than observed and that the fastest winds are greater than those observed by about

3ms$^{-1}$ in summer and 5ms$^{-1}$ in winter. The distributions of wind direction and vorticity (not shown) are reasonably well simulated. However, from April-July there are too many winds from the north and the east in the climate model (see July in Fig. 5).

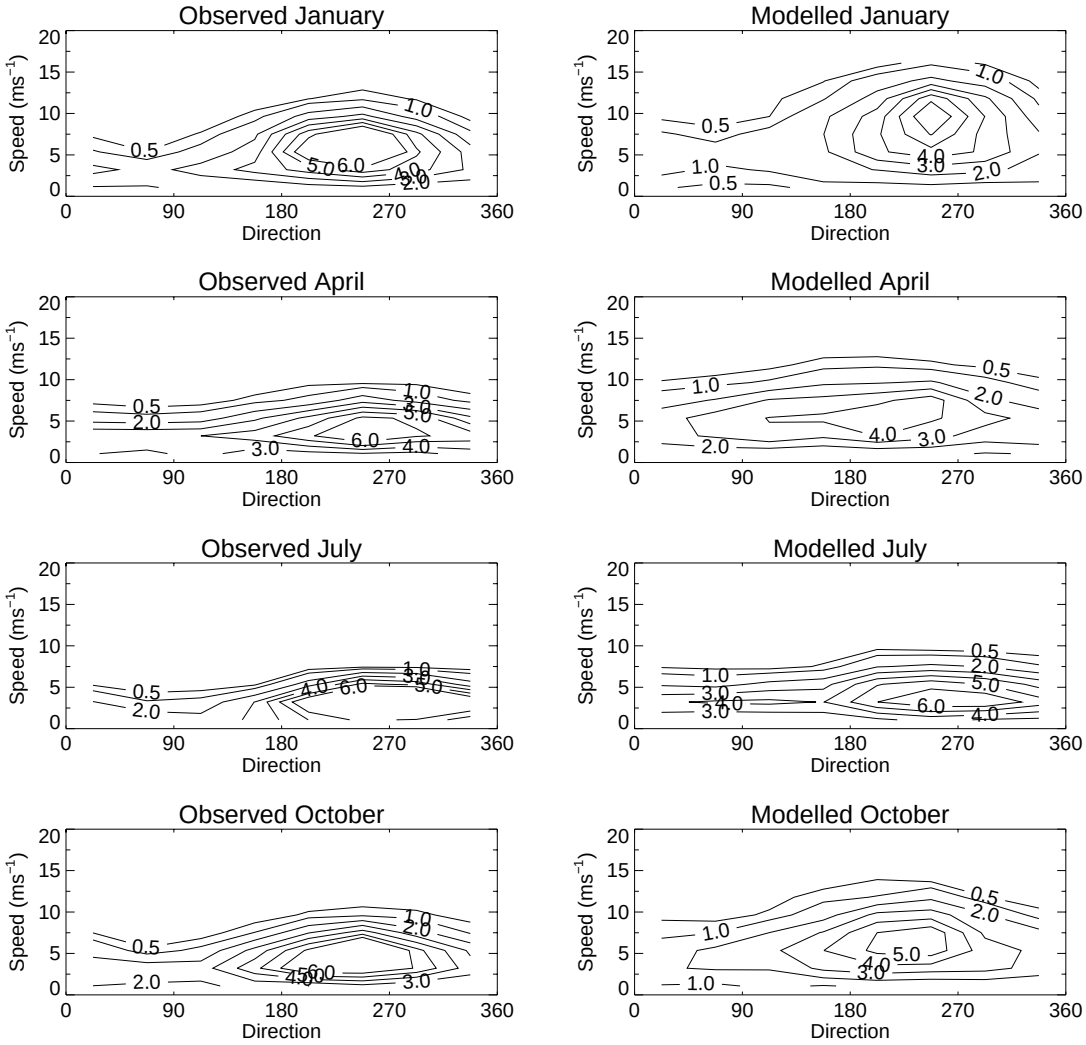


**Figure 5**. *Probability density function (in %) for combinations of wind direction and speed for the second member of the SSTNAT integrations of the HadAM3 model.*

For the modelled data, the best-fit regression surface of CET against circulation from the second member of SSTNAT was used to estimate residuals for the other model integrations. Table 2 shows that warming trends in CET residuals were clearly underestimated by SSTNAT. The observed warming of 0.056°C/decade since 1900 in annual mean CET residuals is above the range of the six individual simulations contributing to SSTNAT (not shown), and the difference in trends (0.018°C/decade) is statistically significant at the 5% level. The annual mean trends from GSOT and GSOTI are closer to the observed value,

suggesting that the direct influence of anthropogenic forcings (Sexton et al. 2001) is required to explain the recent rise in CET. In particular, GSOT and GSOTI simulated the recent high-summer warming well.

**Table 2**. *Comparison of observed and modelled trends ($^{o}$C/decade) in CET residuals for the period 1900-1998. Bold trend values are significant at the 5% level.*

| | Observed CET | SSTNAT | GSOT | GSOTI |
|---|---|---|---|---|
| Annual | **.056** | **.038** | **.059** | **.062** |
| Winter half | **.053** | .032 | **.043** | **.055** |
| Summer half | **.060** | **.042** | **.077** | **.072** |
| High summer | **.086** | **.044** | **.084** | **.084** |

Fig. 6 shows the lowess estimate of the best-fit surface from the second member of SSTNAT. Fig. 6 shows that the model is capturing the combined effect of speed and wind direction on CET reasonably well (compare with Fig. 1) but that the effect of vorticity in the model is too large. In particular, there is too much cooling in anticyclonic conditions. Cyclonic situations in January are generally too warm in the model. In January, the modelled westerlies are too cool whilst in July and October the simulated northerlies and easterlies for neutral and cyclonic vorticity are generally too warm. In December, the northerlies are too cold. Because we use anomalies about the model climatology, these results represent relative errors, not absolute errors in CET.

Figs. 7 and 8 compare modelled and observed time series of anomalies and residuals respectively. The grey shading centred on the observed time series is $\sqrt{1+1/6}$ x 1.96 x the intra-ensemble standard deviation of SSTNAT. This effectively represents the combined 95% confidence level of the observed time series and a six-member ensemble mean. Therefore, if the model time series are outside the grey area, then the observations and model time series are locally significantly different at the 5% level. The confidence intervals are narrower for the residuals than the anomalies, particularly in winter. There is less difference between the anomaly and residual time series in Figs. 7 and 8 than those previously shown by Osborn and Jones (2000). For mean CET anomalies, SSTNAT significantly underestimates the observed warming in the 1990's, especially in the winter half of the year and high summer, whilst both

GSOT and GSOTI simulate CET changes better in this period. The recent discrepancy between SSTNAT and the observations has been slightly reduced by removing the mean circulation effects on CET (Fig. 8). In the 1970's, the three ensemble means underestimate the annual mean CET changes in both the anomaly and residual time series, suggesting that factors other than local circulation are important here.

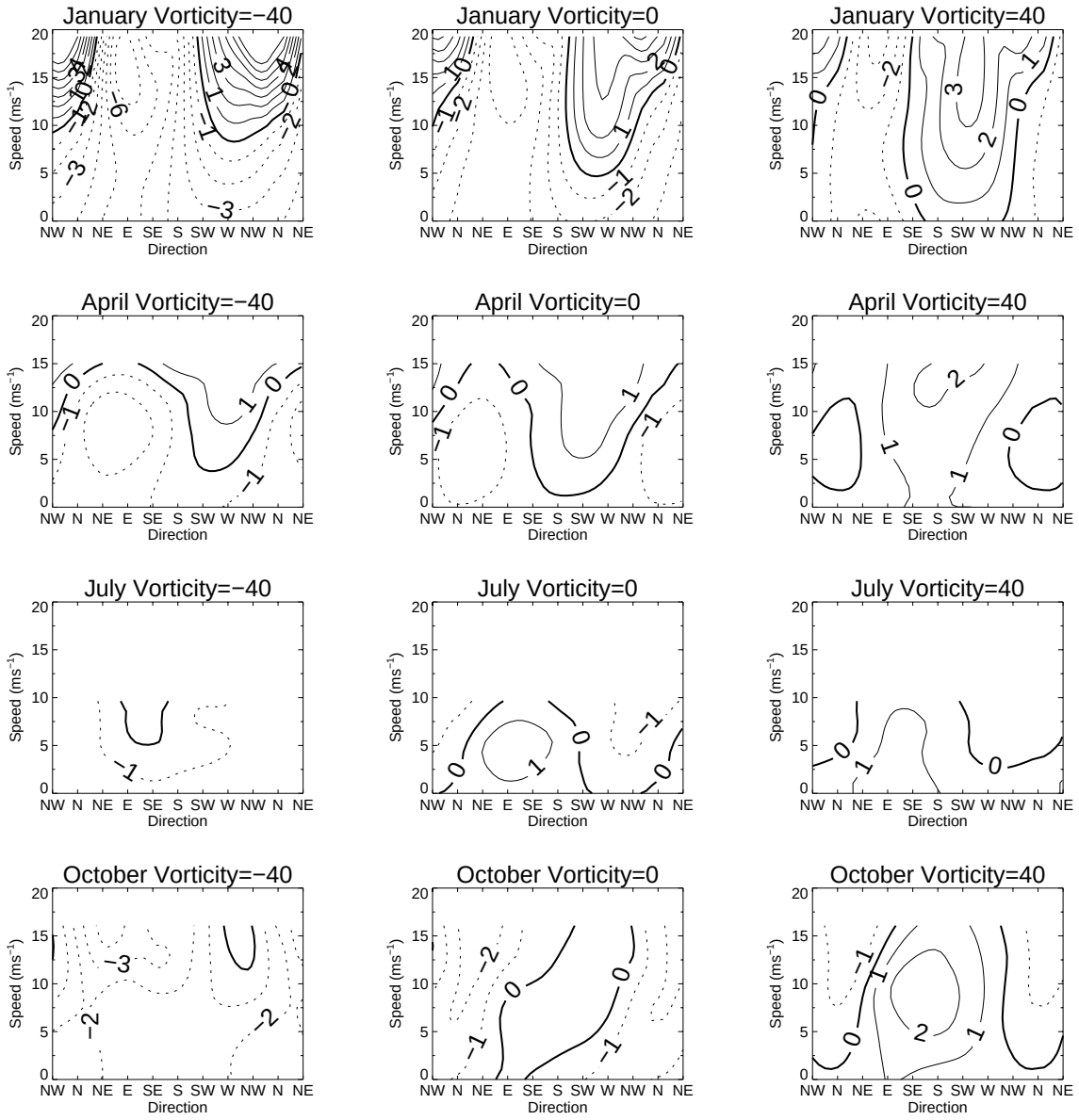


**Figure 6**. *Mean effect of wind direction and speed on CET ($^oC$) for three values of vorticity and for January, April, July and October using the second member of SSTNAT. The smooth regression surface estimated by lowess was sampled for 1ms$^{-1}$ intervals of speed and 40 equally spaced values for wind direction.*

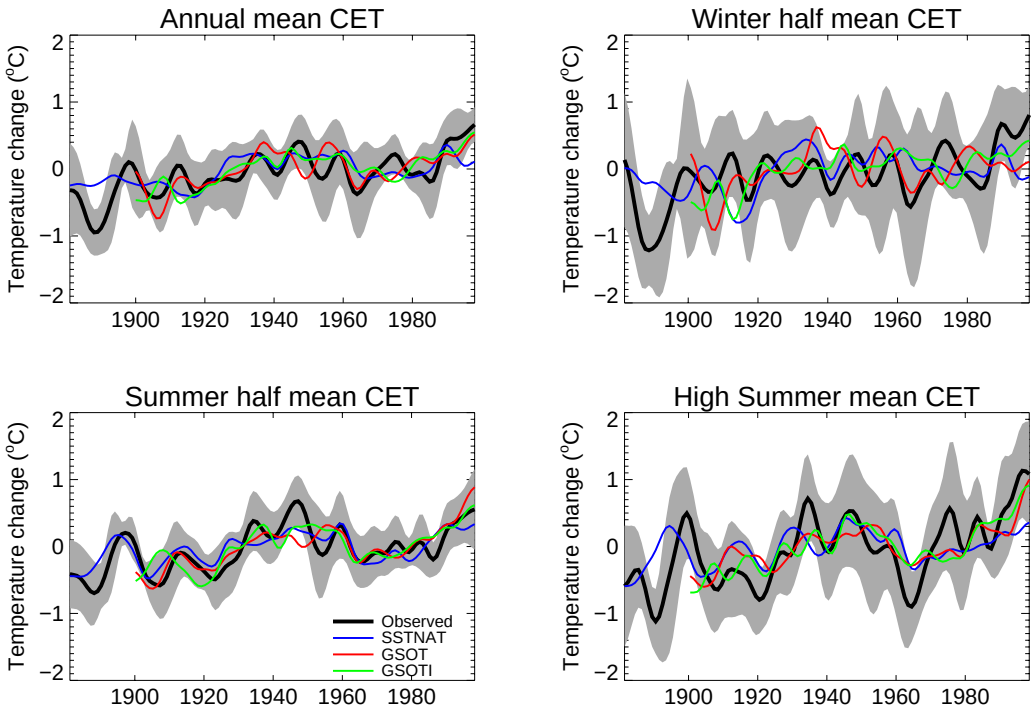


**Figure 7**. *Comparison of low-pass filtered (half power of ~10 years) observed and modelled CET anomalies (°C) from a reference period 1900-1998. Shaded regions are centred on the observed curve and represent the combined 95% confidence level of the observed time series and a six-member ensemble mean.*

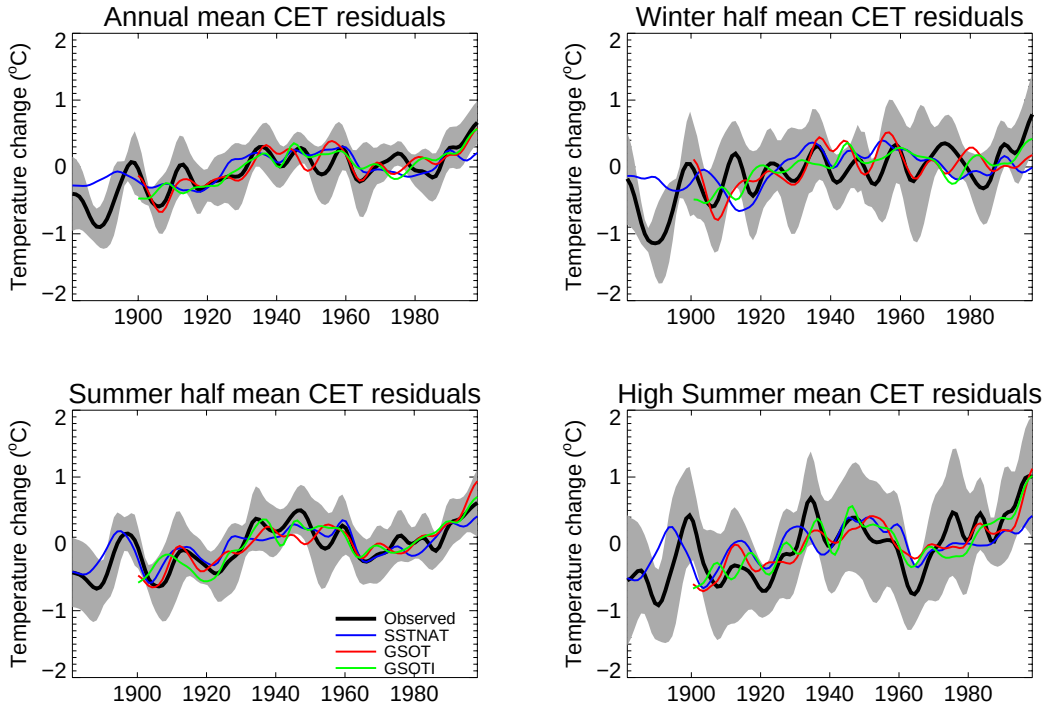


**Figure 8**. *As figure 7 but for CET residuals.*

Many models suggest enhanced continental warming under greenhouse forcing (IPCC, 2001). However, this does not occur in the observed CET since 1966 which shows a warming trend on maritime days (wind direction from 180$^{o}$ through North to 45$^{o}$) of 0.16$^{o}$C/decade relative to other days. This may reflect relative warming of maritime air masses owing to the very rapid warming of SST (Figure 9) in the extratropical North Atlantic since 1985. This oceanic warming is likely to exceed warming from anthropogenic influences alone and seems to be related in part to natural multidecadal fluctuations (Mann and Park 1996), possibly in the thermohaline circulation (Delworth and Mann 2000). Similarly, in the model there was no significant warming during 1966-1998 on continental days relative to maritime days. For 1900-1998, neither model ensembles nor observations showed any significant overall trend of temperatures on continental relative to maritime days.

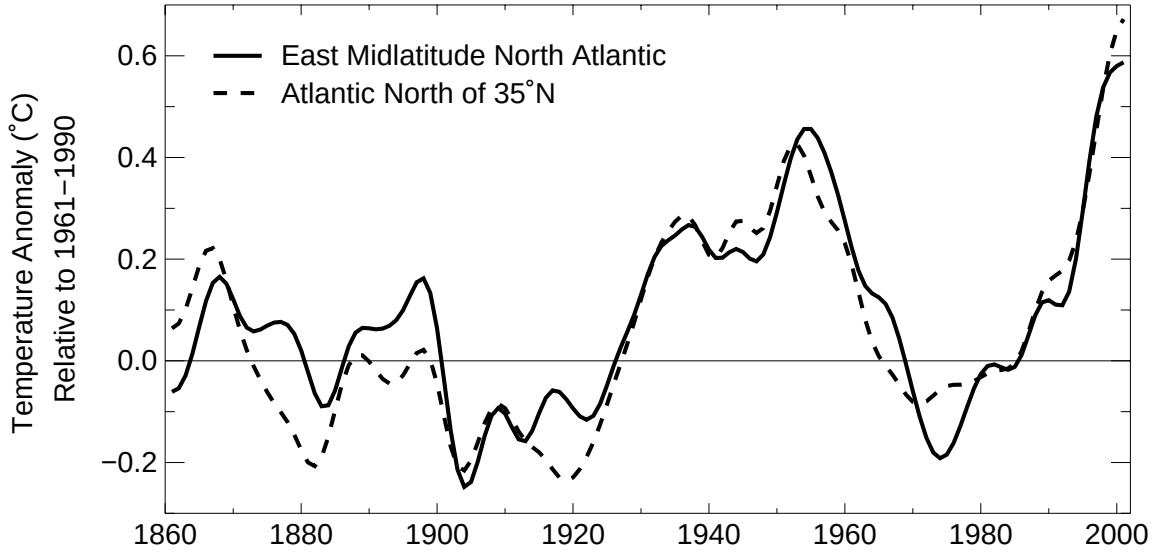


**Figure 9**. *Annual SST, relative to 1961-1990, in the east mid-latitude North Atlantic (~35°-65°N, 0°-35°W) and North Atlantic north of 35°N, 1861-2001. Near decadal smoothing uses 21-term binomial filter.*

## 6. Objective comparison of observed and modelled time series of residual CET

We estimate the effects of SST, natural and anthropogenic forcings on CET anomalies in HadAM3 using the General Linear Model (GLM) technique of Sexton et al (2003). These results are now based on an extended suite of 48 simulations for all or part of 1900-1998 with

different combinations of the five forcings discussed above. The GLM assumes that simulated changes are a linear combination of "direct" anthropogenic signals (Sexton et al. 2001) and their possible interactions in pairs, superimposed on natural signals and an SST effect that implicitly includes anthropogenic influences on SST. A stepwise selection algorithm is used to eliminate statistically insignificant forcings. The end product from the GLM analysis is an estimate of a set of parameters and their standard errors; there is a different parameter for the SSTNAT (combined SST and natural forcings) effect in each year, and a single parameter for each significant anthropogenic effect and for each significant interaction. The time profile of the response to each anthropogenic effect is its annual global-average radiative forcing scaled by its parameter estimate. Likewise the evolution of the interaction between two anthropogenic effects is the product of the two global radiative forcings multiplied by the corresponding parameter estimate. *Modelled* annual CET anomalies (see Fig. 10) were best fitted by a combination of SST and natural forcings (SSTNAT), greenhouse gases (G), the indirect effects of tropospheric aerosols (I), and the interaction between G and I (called GI in Fig. 10). The direct aerosol effect (S) also made a small but statistically significant contribution (not shown). No significant effects due to changing stratospheric and tropospheric ozone (O, T) were detected.

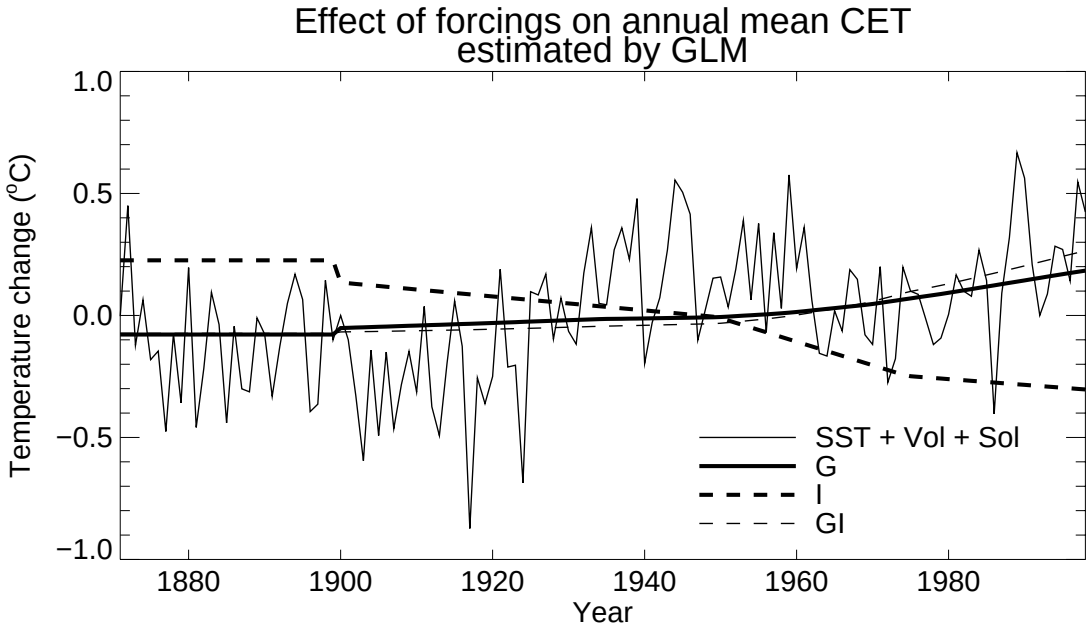


**Figure 10**. *Effect of changing SST + volcanic aerosol + solar output (SST+vol+sol), increasing greenhouse gases (G), indirect aerosol effect (I) and the interaction between G and I (GI) on annual mean CET anomalies (°C) estimated by a General Linear Model.*

To objectively assess which combination of forcing factors best describes the *observed* changes in CET, we first used a technique that is similar to optimal fingerprint detection (Allen and Tett 1999) but adapted for single time series. We regressed various combinations of the four response curves in Fig. 10 onto the observed CET anomalies to determine the linear combination of forcing factors that best describes the observed CET anomalies. The error terms were modelled as a 1st order autoregressive model to account for red noise in CET. Annual mean CET residuals were best described by $(1.003 \pm 0.27) \times \mathrm{SSTNAT} + (1.195 \pm 1.15) \times \mathrm{G}$, where the ranges indicate the 90% confidence intervals of both amplitude estimates. As these 90% confidence intervals overlap with unity but not with zero, the combined simulated effect of SSTNAT and G are consistent with the observations. Out of the other possible combinations of forcing factors, only SSTNAT alone provided a consistent explanation of changes in annual mean CET anomalies. For MAM, AMJJAS, and SON, SSTNAT was the only consistent explanation of the observed CET anomalies. DJF was best described as red noise. For JJA and JA, the amplitudes of the SSTNAT signal were statistically significantly greater than 1. An SSTNAT effect was detected in ONDJFM but the modelled signal was too large (amplitude less than 1).

For the annual means, it is possible that the anthropogenic effects are fitted to variations in CET anomalies that were actually due to variations in local circulation. To test this, the previous analysis was repeated with modelled and observed CET residuals. Both SSTNAT and SSTNAT+G were consistent with the observed annual CET residuals, suggesting that increasing greenhouse gas levels were playing an important role. This was also the case for SON. In contrast with the anomaly analysis, SSTNAT was consistent with the observations for JJA and high summer (JA). This indicates that circulation changes, which have not been reproduced by the climate model, have had an important effect on the observed CET changes in these two seasons. For MAM, the amplitude of the SSTNAT signal estimated to best fit the observed curve was too large so that the 99% confidence interval was neede to overlap with 1.

A problem for this fingerprint approach is that the time series of the modelled response to the various forcing factors (see Fig. 10) that are fitted to the observations are highly correlated with each other. This makes it difficult for the regression to distinguish between the different forcing factors, especially when 3 or more forcing factors are being fitted to the observations. This problem is exacerbated here as we are only considering single time series, whereas other studies e.g. Stott et al., (2000) can use seasonal spatial patterns to reduce the correlation between forcings.

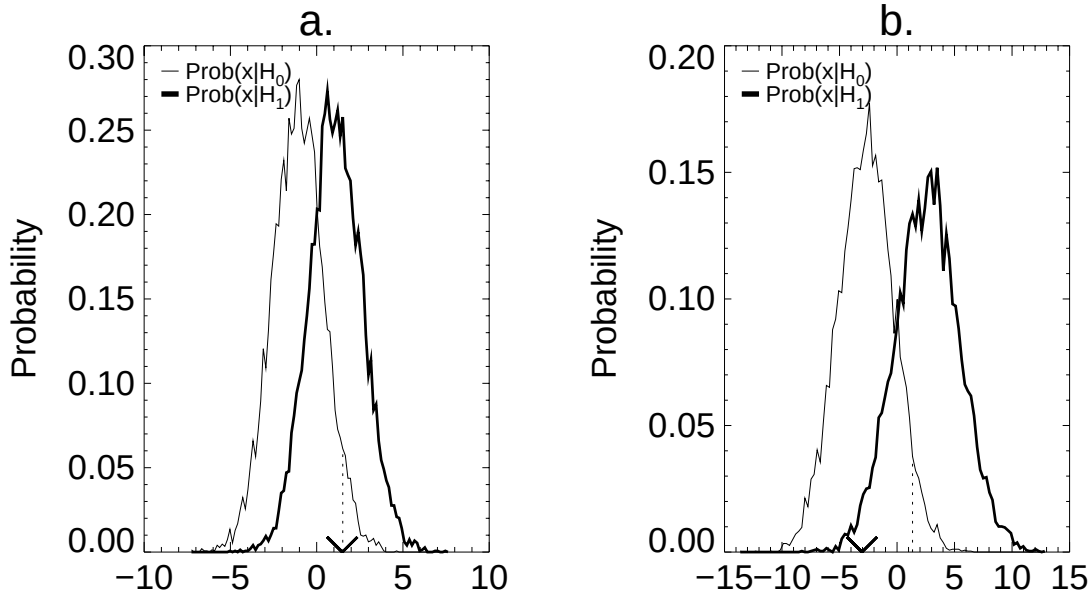


**Figure 11**. *Distributions of log-likelihood ratio test statistic comparing a)* $H_0$*:obs=SSTNAT and* $H_1$*:obs=SSTNAT+G, and b)* $H_0$*:obs=SSTNAT+G and* $H_1$*:obs=SSTNAT+G+S+I+GI, for annual mean CET anomalies. The '∨' symbol on the x-axis indicates the log-likelihood ratio of the observed annual mean CET anomalies. The dashed vertical line in the distribution of* $\mathrm{Prob}(\mathbf{x} \mid H_0)$ *indicates the threshold for a significance level of 5%.*

An alternative to the fingerprint approach is the method of hypothesis testing. Kheshgi and White (2001) describe a Monte Carlo approach to test which of two alternate hypotheses, for which the probability functions have been fully specified, best describes the observed data (see section b in the Appendix). Here, we use the hypothesis tests to determine which combinations of forcings best represent the observed changes in CET. The assumption is that the modelled response of CET to each of the various forcings is realistic; this is a large assumption to make but it overcomes the problem of distinguishing between forcing factors whose effects are highly correlated in time. To test these hypotheses, we use the estimates of parameters and their standard errors produced by the GLM analysis, to fully define the probability distribution of data for each combination of forcings. These distributions are then used in the Monte Carlo approach to synthetically produce time series consistent with a given set of forcings. Section b in the Appendix describes the methodology in more detail.

Fig. 11 shows the results for annual mean CET anomalies produced by the Monte Carlo approach. The thin (thick) curve shows the PDF of the likelihood ratio of data coming from

$H_1$ rather than $H_0$ given that the data have been generated by $H_0$($H_1$). The '$\vee$' symbol shows the likelihood ratio of the observations. In Fig. 11a, '$\vee$' lies within the PDF for $\mathrm{Prob}(\mathbf{x} \mid H_1)$ and just beyond the 5% significance level (the vertical dashed line) of the PDF of $\mathrm{Prob}(\mathbf{x} \mid H_0)$. This indicates that the observed annual mean CET is significantly more consistent with SSTNAT+G than with SSTNAT or, SSTNAT+G+S+I+GI (Fig. 11b), andor a red noise process (not shown). Therefore SSTNAT+G is the best simulation of the observed annual mean CET, a result that could not be established by the fingerprint analysis above. For MAM, JJA, and SON, SSTNAT and SSTNAT+G could not be distinguished and were equally good explanations of the observed time series. In DJF the changes in CET were best described as red noise, using the serial correlation estimated in the GLM analysis. The hypothesis test was not applied to the CET residuals because the Monte Carlo procedure is more complicated as we would also be required to replicate the lowess estimation of the local circulation effects on CET and their subsequent removal from the anomalies to generate residuals. Another way of thinking about this is that the circulation effects themselves have uncertainties and that these uncertainties are present in the residuals. Therefore any detection strategy based on residuals must account for this hidden uncertainty or risk erroneously obtaining too many significant results.

## 7. Conclusions

Our analysis of CET since the late 19$^{th}$ century shows that its long-term warming cannot be fully explained by atmospheric circulation changes, natural forcings and rising SST alone, though the non-linear behaviour of SST in the North Atlantic since 1880, including its most recent warming, is clearly influential. The lack of warming of CET on light-wind nights relative to other nights indicates that CET is unlikely to be significantly affected by urbanization.

The regression analysis suggests a significant human influence from increasing greenhouse gases on CET in the observations. We also used hypothesis tests, which can cope with several highly correlated anthropogenic effects, but do so at the expense of assuming the simulated response to each forcing factor is realistic. These hypothesis tests confirmed that a combination of SST, natural forcings and increasing greenhouse gases best describes the annual mean observed changes in CET from 1881-1998. This reduces the possibility that the result from the regression analysis was due to limitations in the technique for distinguishing

between highly correlated anthropogenic effects. However, the conclusions are tentative ones because the results are only significant for the full period. As the prescribed SST forcing already contains some human influence, we cannot rule out effects from anthropogenic forcings other than increasing greenhouse gases.

## Appendix

### a. Locally weighted regression

Local weighted regression, or lowess, is a multivariate procedure for fitting a non-parametric regression surface to a set of data allowing for a wide variety of linear or non-linear responses (Cleveland and Devlin 1988). The method is very flexible allowing for a wide range of possible surfaces to be fitted to the data.

In the univariate case, where we have *N* dependent data, $y_i$, and an explanatory variable, $x_i$, for i=1,…,*N*, we model the data as consisting of some unknown function of the explanatory data, $g(x_i)$ plus some unexplained variation, $e_i$. Locally weighted regression estimates $g(x_i)$ are made as follows. For each value of $x_i$, say X, we form a subset of the $x_i$'s which are closest in value to X, such that the subset covers a specified fraction of $x_i$, called the *span*. To estimate $g(X)$, we regress this subset of $x_i$ against the corresponding values of $y_i$ using a weighted linear or quadratic regression. The weights, $w_i$, are calculated using a *tri-cube* function (Eqn. 1) of the distance between the $x_i$'s and X divided by the maximum distance between the $x_i$'s and X in the subset. The *tri-cube* function is used as it has a very smooth contact with 0 and 1, which ensure that the locally weighted regression behaves well.

$$w_i = \left[ 1 - \left( \frac{|x_i - X|}{\max |x_i - X|} \right)^3 \right]^3 \qquad \text{Eqn 1}$$

The procedure ensures that the best fit, $\hat{g}(x_i)$, is a linear combination of the data, $y_i$. To enable standard errors for the predicted values to be estimated, we assume that the error terms, $e_i$, are Gaussian and have constant variance.

A number of key statistics are produced by lowess, which are described in detail in Cleveland and Devlin (1988). The variance of the residuals, $\hat{e}_i = y_i - \hat{g}(x_i)$, measures the precision of the fit. The number of equivalent parameters, $N_p$, effectively measures the smoothness of the fit. For prediction, it is desirable to keep $N_p$ to a minimum otherwise the standard errors of the predicted values become large rendering the prediction useless. However, a downside of over-smoothing is that bias, which is the difference between the best fit, $\hat{g}(x_i)$, and the true response, $g(x_i)$, is increased, unless the true response is a simple polynomial relationship of degree no more than that used in the lowess fit. The smoothness of the best fit is partly a property of the data but also depends on the span and degree of the local fit chosen by the analyst. As the span is increased or the degree reduced, $N_p$ decreases and the bias increases.

Cleveland and Devlin (1988) provide a method, which is implemented in S-Plus, to guide the choice of the span and degree so that there is a balance between $N_p$ and the bias. This approach uses Mallow's $C_p$ statistic to measure the combined amount of smoothness and bias. Despite the objectivity of this approach, Cleveland and Devlin advise that the final choice of span depends on the application. For instance, if a simple relationship between $x_i$ and $y_i$ is sought, then over-smoothing is desirable and a large bias can be tolerated. This approach can also be used to determine whether some explanatory variables are redundant.

Cleveland and Devlin (1988) also generalise the univariate technique to cope with $p$>1 explanatory variables. For the case with two explanatory variables, $x_i$ and $z_i$, and where the degree of the lowess estimate is 2, the local polynomial regression is of the form

$$y_i = \alpha(x - x_i) + \beta(z - z_i) + \gamma(x - x_i)^2 + \delta(z - z_i)^2 + \eta(x - x_i)(z - z_i) + e_i . \qquad \text{Eqn 2}$$

The inclusion of the term $\eta(x - x_i)(z - z_i)$ enables lowess to cope with non-linear interactions between the two explanatory variables. The weighting function depends on the distance between the $p$-element vectors $\mathbf{x_i}$ and $\mathbf{X}$ in $p$-dimensional space. The major practical consideration is that the $p$ explanatory variables may have different scales. To prevent any single explanatory variable dominating the calculation of distance, the explanatory variables are normalised by a measure of their scale; we used the inter-quartile range rather than the standard deviation as it is more robust. Was the original or the extended wind direction

datasetyou describe below used to calculate the “inter-quartile range” of wind direction? If the latter, which parts of it?

A weakness of the standard lowess technique is that it does not allow for cyclic explanatory variables such as wind direction. Thus values of wind direction such as $1^o$ and $359^o$ are not treated as local. As the standard software does not deal with cyclic variables, we used the following procedure to approximately allow for the periodicity of wind direction. First, we determined the scale for each of the explanatory variables. We then formed a new set of data by subtracting 360 from the original wind directions; wind directions in this set could not exceed $0^o$. Likewise, we formed another set by adding 360 to the wind directions. These two sets were joined with the original data set, and each explanatory variable was normalised by its appropriate scale to form a combined set that was used for the lowess estimation. This larger data set ensured that data with wind directions either side of $0^o$ were treated as ‘local’ in lowess. Only the regression surface for wind directions between $0^o$ and $360^o$ was used for subsequent prediction.

**b. Hypothesis testing**

Hypothesis tests can be used to determine which of two hypotheses, called the null ($H_0$) and the alternative ($H_1$), best describes some data, $\mathbf{y}$. Both hypotheses must have fully defined probability distributions, $P_0(\mathbf{y})$ and $P_1(\mathbf{y})$ respectively. Two types of error are possible in hypothesis testing. So-called Type I errors occur when $H_0$ is falsely rejected when it is true. Type II errors are when $H_1$ is wrongly accepted when it is false. The probability of a type I error occurring, which is called the *significance level*, $\alpha$, can be specified prior to the hypothesis test. The probability of a type II error not occurring, $1-\beta$, is called the *power of the test* and it is desirable to maximise this.

Neyman and Pearson defined the test statistic for which the power is maximised given a specified significance level (e.g. Kendall and Stuart 1977). This test statistic, which provides the optimal test to decide between the two hypotheses, is the likelihood ratio statistic,

$$L(\mathbf{y}) \equiv P_1(\mathbf{y}) / P_0(\mathbf{y}) \equiv P(\mathbf{y} \mid H_1) / P(\mathbf{y} \mid H_0) . \qquad \text{Eqn 3}$$

The most powerful test of whether $H_1$ best describes the data is if

$$L(\mathbf{y}) > \theta , \qquad \text{Eqn 4}$$

where $\theta$ is some ‘threshold’ value of likelihood-ratio statistic to be determined.

The hypothesis test is then a three-step process, which is outlined here but is presented in more detail in Kheshgi and White (2001):

1. Derive two likelihood ratio functions based on the statistical models for $H_0$ and $H_1$. These two likelihood functions can be written as $P(L \mid H_0)$ and $P(L \mid H_1)$.

2. Specify the significance level, $\alpha$, and determine the threshold, $\theta$, by the relationship,

$$\alpha = P(L > \theta \mid H_0) \qquad \text{Eqn 5}$$

The relationship between $\theta$ and the power, $1-\beta$, is

$$1-\beta = P(L \le \theta \mid H_1). \qquad \text{Eqn 6}$$

3. Apply the test to the data to determine $L(\mathbf{y})$ and test Eqn. 4. Four outcomes are possible: $H_0$ or $H_1$ is accepted in favour of the other hypothesis, or both hypotheses are rejected, or neither hypothesis is accepted in favour of the others.

Step one is the most complicated part of the algorithm. Kheshgi and White (2001) describe a Monte Carlo approach to estimate $P(L \mid H_0)$ and $P(L \mid H_1)$. Here, we describe the Monte Carlo approach used in this study.

The two hypotheses we test are whether the observed time series is best represented by the climate model forced by two different combinations of forcing factors. A General Linear Model (GLM) (Sexton 2001) (Eqn 7) has been used to estimate the effects of the various forcing factors in the climate model, and it can be used to describe the probability function of data coming from any combination of these forcings (see Eqn 8).

$$\mathbf{y} = \mathbf{X}\boldsymbol{\beta} + \boldsymbol{\varepsilon}, \quad \text{where } \boldsymbol{\varepsilon} \sim N(\mathbf{0}, \sigma^2 \mathbf{V}(r)), \qquad \text{Eqn 7}$$

where $\mathbf{y}$ is the CET data from all integrations joined together, $\boldsymbol{\varepsilon}$ is the noise component with variance, $\sigma^2$, and a correlation matrix, $\mathbf{V}$, specified by a AR(1) process with lag-1 correlation, $r$. $\boldsymbol{\beta}$ is the vector of parameters which represent the SSTNAT and anthropogenic effects. For SSTNAT, there is a parameter in $^{o}$C for each time point in the modelled temperature data. There is a single parameter for each anthropogenic effect, and this is multiplied by the global radiative forcing (see below) to produce an estimate of the temperature response to that forcing. Each element of $\boldsymbol{\beta}$ has its own Gaussian distribution based on the estimate and standard error from the GLM analysis, and this can be used to

randomly generate vectors like $\boldsymbol{\beta}$, called $\boldsymbol{\beta}_{rand}$. $\mathbf{X}$ is a matrix of coefficients that describe how each element of $\mathbf{y}$ is related to each parameter of $\boldsymbol{\beta}$. For SSTNAT parameters, the corresponding columns of $\mathbf{X}$ consist of 0's and 1's. For an anthropogenic parameter the corresponding column of $\mathbf{X}$ consists of values of global radiative forcing if the corresponding elements of $\mathbf{y}$ come from integrations that include this forcing, or otherwise 0. Therefore, $\mathbf{X}$ depends on the design of the experiment.

The probability of any data arising from the GLM is defined by

$$P_{GLM}(\mathbf{y}) = (2\pi)^{-n/2} \left|\mathbf{V}\right|^{-1/2} \exp\left\{-\frac{1}{2}(\mathbf{y}-\mathbf{X}\boldsymbol{\beta})^T \mathbf{V}(r)^{-1}(\mathbf{y}-\mathbf{X}\boldsymbol{\beta})\right\}, \qquad \text{Eqn 8}$$

where n is the number of points in $\mathbf{y}$.

To estimate $P(L \mid H_0)$ with a Monte Carlo approach, we use Eqn 9 to produce a randomly generated time series, $\mathbf{y}_{rand}$, based on the GLM estimates for the combination of forcings in $H_0$. First, $\boldsymbol{\beta}_{rand}$ was randomly generated and all elements corresponding to forcings not included in the combination of forcings in $H_0$ were set to zero. Then $\mathbf{X_0}$ is created in the same way as $\mathbf{X}$ but as if it were for a single integration with the forcings in $H_0$. In effect, the parameters of $\boldsymbol{\beta}_{rand}$ that correspond to SSTNAT effects produce a randomly generated time series of the model response to SSTNAT forcing. Also, a randomly generated time series of the model response to a particular anthropogenic forcing is made by multiplying the time profile of its global radiative forcing by the appropriate parameter in $\boldsymbol{\beta}_{rand}$. Randomly generated curves are produced for each anthropogenic forcing and interaction in $H_0$ and added together to the random SSTNAT series. The stochastic component, $\boldsymbol{\varepsilon}_{rand}$, was generated as a random Markov process with noise variance, $\sigma^2$, and lag-1 correlation, $r$. Then

$$\mathbf{y}_{rand} = \mathbf{X_0}\boldsymbol{\beta}_{rand} + \boldsymbol{\varepsilon}_{rand}. \qquad \text{Eqn 9}$$

Eqn. 8 defines the probability of $\mathbf{y}_{rand}$ occurring under the GLM for each of the two hypotheses, $P_0(\mathbf{y_{rand}})$ and $P_1(\mathbf{y_{rand}})$. Eqn. 3 is used to estimate $L(\mathbf{y_{rand}})$. To estimate $P(L \mid H_0)$, this procedure was repeated 1000 times to provide 1000 estimates of $L(\mathbf{y_{rand}})$. Step one is completed by estimating $P(L \mid H_1)$ in a similar way using synthetic time series based on the GLM estimates of the combination of forcings in $H_1$.

**Acknowledgments**

The UK Dept. of the Environment, Food, and Rural Affairs (Contract PECD/7/12/37) and the UK Government Meteorological Research Program funded this work. This paper is British Crown Copyright. The earlier work on CET residuals that inspired this analysis was done by Peter Wright under contract Met 16/2068. Briony Horton, Ian Macadam and Mark Rodwell made supporting computations. Thanks to Peter Stott and Michael Mann for comments on this paper. Thanks to William Cleveland, Eric Grosse, and Ming-Jen Shyu for making the locally weighted regression software freely available on the web at http://cm.bell-labs.com/cm/ms/departments/sia/wsc/smoothsoft.html.

**References**

Allen, M. R. and S. F. B. Tett, 1999: Checking for model consistency in optimal finger printing. *Clim. Dyn.*, **15**, 419-434.

Braganza, K., D. J. Karoly, A. C. Hirst, M. E. Mann, P. Stott, R. J. Stouffer, and S. F. B. Tett, 2003: Simple indices of global climate variability and change: Part I - variability and correlation structure. *Clim. Dyn.*, **20**, 491-502.

Cleveland, W. S. and S. J. Devlin, 1988: Locally weighted regression: an approach to regression analysis by local fitting. *J. Amer. Stat. Assoc*., **83** (403), 596-610.

Delworth, T. L. and T. R. Knutson, 2000: Simulation of early 20$^{th}$ century global warming. *Science,* **287**, 2246-2250.

Delworth, T. L. and M. E. Mann, 2000: Observed and simulated multidecadal variability in the Northern Hemisphere. *Clim. Dyn.*, **16** (9), 661-676.

Diggle, P. J., K.-Y. Liang, and S. L. Zeger, 1999: *Analysis of longitudinal data,* Clarendon Press, Oxford, 253pp.

Easterling, D.R., E. B. Horton, P. D. Jones, T. C. Peterson, T. R. Karl, D. E. Parker, M. J. Salinger, V. N. Razuvayev, N. Plummer, P. Jamason, and C. K. Folland, 1997: Maximum and minimum temperature trends for the globe. *Science, **277***, 364-367.

Folland, C. K., 1983: Regional-scale interannual variability of climate - a north-west European perspective. *Met. Mag*., **112**, 163-183.

Folland, C. K., D. M. H. Sexton, D. J. Karoly, C. E. Johnson, D. P. Rowell, and D. E. Parker, 1998: Influences of anthropogenic and oceanic forcing on recent climate change. *Geophys. Res. Lett.,* **25,** 353-356.

Gillett, N. P., G. C. Hegerl, M. R. Allen and P. A. Stott, 2000: Implications of changes in the Northern Hemisphere circulation for the detection of anthropogenic climate change. *Geophys. Res. Lett.,* **27**, 993-996.

Hurrell, J. W., 1995: Decadal trends in the North Atlantic Oscillation: regional temperatures and precipitation. *Science*, **269**, 676-679.

Hurrell, J. W., M. P. Hoerling, and C. K. Folland, 2001: Climate variability over the North Atlantic, *Meteorology at the Millennium*, ed: R. Pearce, Academic Press, London, 143-151.

Houghton, J. T., Y. Ding, D. J. Griggs, M. Noguer, P. van der Linden, X. Dai, K. Maskell and C. I. Johnson, Eds., 2001: *Climate Change 2001: The Scientific Basis, Contribution of Working Group I to the Third Assessment Report of the Intergovernmental Panel on Climate Change*. Cambridge Univ. Press, 881 pp.

Jenkinson, A. F., and P. Collison, 1977. An initial climatology of gales over the North Sea. *Synoptic Climatology Branch Memorandum*, **62**. Met Office, UK, 18 pp.

Johns, T. C., J. M. Gregory, W. J. Ingram, C. E. Johnson, A. Jones, J. F. B. Mitchell, D. L. Roberts, D. M. H. Sexton, D. S. Stevenson, S. F. B. Tett, and M. J. Woodage, 2001. Anthropogenic climate change for 1860 to 2100 simulated with the HadCM3 model under updated emissions scenarios. *Hadley Centre Technical Note 22*, Met Office.

Johnson, G. T., T. R. Oke, T. J. Lyons, D. G. Steyn, I. D. Watson and J. A. Voogt, 1991: Simulation of surface urban heat islands under 'ideal' conditions at night., Part I: Theory and tests against field data. *Bound. Lay. Meteorol.,* **56**, 275-294.

Jones, P. D., E. B. Horton, C. K. Folland, M. Hulme, D. E. Parker and T. A. Basnett, 1999: The use of indices to identify changes in climatic extremes. *Clim. Change*, **42**, 131-149.

Jones, P. D., M. Hulme and K. R. Briffa, 1993: A comparison of Lamb circulation types with an objective classification scheme. *Int. J. Climatol.,* **13**, 655-663.

Kendall, M. G., and Stuart, A., 1977: *The advanced theory of statistics. Volume 2. Inference and relationship.* Charles Griffin and Company, 748pp.

Khesghi, H. S. and B. S. White, 2001: Testing distributed parameter hypotheses for the detection of climate change. *J. Climate*, **14**, 3464-3481.

Lean, J., J. Beer and R. Bradley, 1995: Reconstruction of solar irradiance since 1610: Implications for climate change. *Geophys. Res. Lett.*, **22**, 3195-3198.

Mann, M. E. and J. Park, 1996: Joint spatiotemporal modes of surface temperature and sea level pressure variability in the Northern Hemisphere during the last century. *J. Clim.*, **9**, 2137-2162.

Osborn, T. J., D. Conway, M. Hulme, J. M. Gregory, and P. D. Jones, 1999: Air flow influence on local climate: observed and simulated mean relationships for the United Kingdom. *Climate Research*, **13**, 173-191.

Osborn, T. J., and P. D. Jones, 2000: Air flow influences on local climate: observed United Kingdom climate variations. *Atmospheric Science Letters*, **1**, 62-74.

Parker, D. E., T. P. Legg and C. K. Folland, 1992: A new daily Central England Temperature series, 1772-1991. *Int. J. Climatol.*, **12**, 317-342.

Pope, V. D., M. L. Gallani, P. R. Rowntree and R. A. Stratton, 2000: The impact of new physical parametrizations in the Hadley Centre climate model HadAM3, *Clim. Dyn.*, **16**, 123-146.

Rayner, N. A., E. B. Horton, D. E. Parker, C. K. Folland and R. B. Hackett, 1996: Version 2.2 of the Global sea-Ice and SST data set, 1903-1994. *Hadley Centre Technical Note no.* **74**, Met Office.

Rodwell, M.J. and C.K. Folland**,** 2003: Atlantic air-sea interaction and model validation. *Annals of Geophysics*, **46**, 47-56.

Sato, M., J. E. Hansen, M. P. McCormick and J. B. Pollack, 1993: Stratospheric aerosol optical depths 1850-1990. *J. Geophys. Res.*, **98**, 22,987-22,994.

Sexton, D. M. H., H. Grubb, K. P. Shine, and C. K. Folland, 2003: Design and analysis of climate model experiments for the efficient estimation of anthropogenic signals, *J. Climate*, **16**, 1320-1336.

Sexton, D. M. H., D. P. Rowell, C. K. Folland, and D.J. Karoly, 2001: Detection of anthropogenic climate change using an atmospheric GCM. *Clim. Dyn.*, **17**(9), 669-685.

Shindell, D. T., R. L. Miller, G. A. Schmidt, and L. Pandolfo, 1999: Simulation of recent northern winter climate trends by greenhouse-gas forcing. *Nature* **399,** 452-455.

Spagnoli, B., S. Planton, M. Déqué, O. Mestre, and J.-M. Moisselin, 2002: Detecting climate change at a regional scale: The case of France, Geophys. Res. Lett., **29**, art. no. 1450.

Stott, P. A. and S. F. B. Tett, 1998: Scale-dependent detection of climate change, *J. Climate*, **11**, 3282-3294.

Stott, P. A., S. F. B. Tett, G. S. Jones, M. R. Allen, J. F. B. Mitchell and G. J. Jenkins, 2000: External control of twentieth century temperature variations by natural and anthropogenic forcings, *Science*, **290**, 2133-2137.

Stott, P. A., 2003: Attribution of regional-scale temperature changes to anthropogenic and natural causes, *Geophys. Res. Lett.*, **30**, art. No. 1728.

Tett, S. F. B., P. A. Stott, M. R. Allen, W. J. Ingram and J. F. B. Mitchell, 1999: Causes of twentieth-century temperature change near the Earth's surface. *Nature*, ***399***, 569-572.

Zwiers, F. W., and X. Zhang, 2003: Toward regional-scale climate change detection, *J. Climate*, **16**, 793-797.

---

D.M.H. Sexton, D.E. Parker, C.K. Folland, Hadley Centre for Climate Prediction and

Research, Met Office, Fitzroy Road, Exeter, Devon, EX1 3PB, UK.

(david.sexton@metoffice.com)